

AperTO - Archivio Istituzionale Open Access dell'Università di Torino

## Impact of the Physicochemical Features of TiO<sub>2</sub>Nanoparticles on Their in Vitro Toxicity

### **This is the author's manuscript**

*Original Citation:*

*Availability:*

This version is available <http://hdl.handle.net/2318/1769066> since 2025-01-23T13:57:30Z

*Published version:*

DOI:10.1021/acs.chemrestox.0c00106

*Terms of use:*

Open Access

Anyone can freely access the full text of works made available as "Open Access". Works made available under a Creative Commons license can be used according to the terms and conditions of said license. Use of all other works requires consent of the right holder (author or publisher) if not exempted from copyright protection by the applicable law.

(Article begins on next page)

## Impact of the Physicochemical Features of TiO<sub>2</sub> Nanoparticles on Their *In Vitro* Toxicity

Ozge Kose<sup>†</sup>, Maura Tomatis<sup>†</sup>, Lara Leclerc<sup>†</sup>, Naila-Besma Belblidia<sup>§,||</sup>, Jean-François Hochepped<sup>§,||</sup>, Francesco Turci<sup>‡</sup>, Jérémie Pourchez<sup>†</sup>, Valérie Forest<sup>\*†</sup>

<sup>†</sup>Ecole de Mines Saint-Etienne, Univ Lyon, Univ Jean Monnet, INSERM, U 1059 Sainbiose, Centre CIS, F-42023 Saint-Etienne, France.

<sup>‡</sup>Dipartimento di Chimica and 'G. Scansetti' Interdepartmental Center for Studies on Asbestos and other Toxic Particulates, Università degli Studi di Torino, Torino, Italy

<sup>§</sup>Mines ParisTech, PSL Research University, MAT - Centre des matériaux, CNRS UMR 7633, BP 87 91003 Evry, France.

<sup>||</sup> ENSTA ParisTech UCP, Institut Polytechnique Paris, 828 bd des Maréchaux, 91762 Palaiseau cedex France.

\* **Corresponding author:** Valérie Forest:

Mines Saint-Etienne, 158 cours Fauriel, CS 62362, 42023 Saint-Etienne Cedex 2. FRANCE.

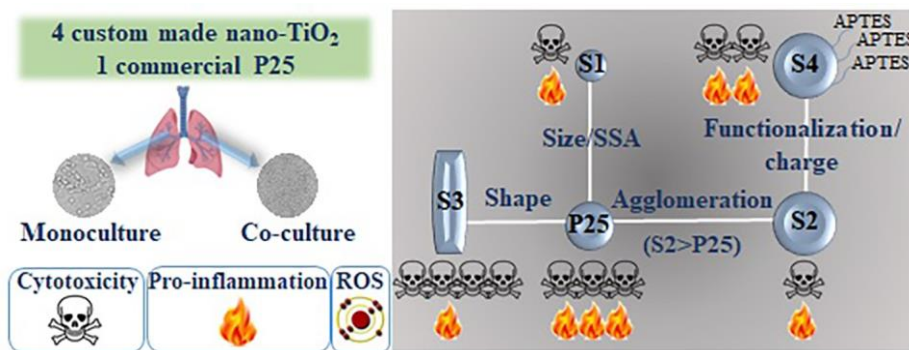
Email: vforest@emse.fr

### Keywords

Titanium dioxide nanoparticles; cytotoxicity; pro-inflammatory response; reactive oxygen species; human lung cells.

**ABSTRACT:**

The concern about titanium dioxide nanoparticles (TiO<sub>2</sub>-NPs) toxicity and their possible harmful effects on human health has increased. Their biological impact is related to some key physicochemical properties, that is, particle size, charge, crystallinity, shape, and agglomeration state. However, the understanding of the influence of such features on TiO<sub>2</sub>-NP toxicity remains quite limited. In this study, cytotoxicity, proinflammatory response, and oxidative stress caused by five types of TiO<sub>2</sub>-NPs with different physicochemical properties were investigated on A549 cells used either as monoculture or in co-culture with macrophages differentiated from the human monocytic THP-1 cells. We tailored bulk and surface TiO<sub>2</sub> physicochemical properties and differentiated NPs for size/specific surface area, shape, agglomeration state, and surface functionalization/charge (aminopropyltriethoxysilane). An impact on the cytotoxicity and to a lesser extent on the proinflammatory responses depending on cell type was observed, namely, smaller, large-agglomerated TiO<sub>2</sub>-NPs were shown to be less toxic than P25, whereas rod-shaped TiO<sub>2</sub>-NPs were found to be more toxic. Besides, the positively charged particle was slightly more toxic than the negatively charged one. Contrarily, TiO<sub>2</sub>-NPs, whatever their physicochemical properties, did not induce significant ROS production in both cell systems compared to nontreated control groups. These results may contribute to a better understanding of TiO<sub>2</sub>-NPs toxicity in relation with their physicochemical features.



## 1. INTRODUCTION

Titanium dioxide ( $\text{TiO}_2$ ) is an inorganic compound, which is widely used in a large range of industrial applications mainly due to its high refractive index or photocatalytic properties.<sup>1,2</sup> World production of  $\text{TiO}_2$  nanoparticles ( $\text{TiO}_2$ -NPs) in 2014 was estimated to exceed 9 million metric tons<sup>3</sup> to be used in many consumer products such as paints (*e.g.*, UV resistant and antibacterial self-cleaning paints), antiseptic-antimicrobial compositions, deodorization (purify/deodorize indoor air), inks, papers, plastics, UV-sunscreen, toothpastes, ceramics, and food products.<sup>3-5</sup> This makes  $\text{TiO}_2$ -NPs one of the most abundantly produced nanomaterials (NMs) showing various forms of shape, crystalline phases, and nano size ranges. As it is the second most used NM in consumer products,<sup>6</sup> the concern about  $\text{TiO}_2$ -NPs toxicity and their possible harmful effects on human health has increased.<sup>7-9</sup>

The toxicity of NPs is greatly related to their interaction with biological systems. This interaction is associated with the physicochemical properties of the NPs.<sup>10</sup> Generally, cellular uptake of NPs is determined by their size, surface area, shape, surface charge, chemical composition, crystallographic phases, and surface modifications.<sup>11</sup> The internalization of NPs through cell membrane might lead to potential hazards by interaction with intracellular biological macromolecules.

Table 1.  $\text{TiO}_2$ -NPs Used in This Study with Their Specific Characteristics

S1	S2	S3	S4	P25
custom-made for size/SSA	custom-made for agglomeration		custom-made for shape custom-made for functionalization/ charge	commercial/used as a reference

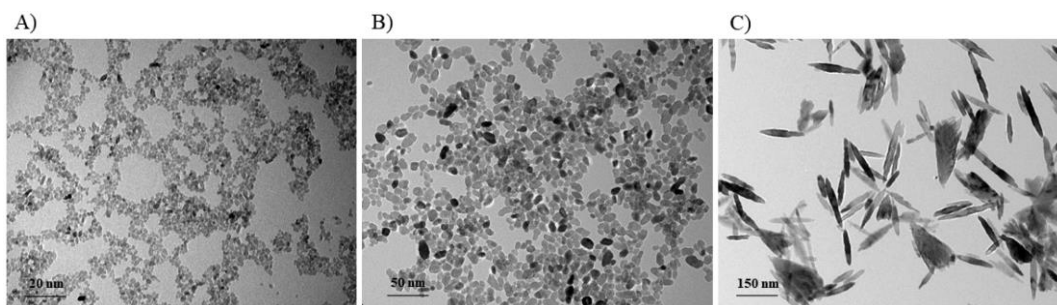


Figure 1. TEM images of  $\text{TiO}_2$ -NPs (A) S1, (B) S2, and (C) S3.

Table 2. Particle Primary Size, SSA, Shape, Average Hydrodynamic Size, Polydispersity Index, and  $\zeta$  Potential in Culture Media (in DMEM) and in Deionized Water (DI H<sub>2</sub>O) after Dispersion of TiO<sub>2</sub>-NPs (120  $\mu$ g/mL)<sup>a</sup>

Primary size (nm)	SSA (m <sup>2</sup> /g)	shape	DI H <sub>2</sub> O			DMEM + 10% FBS		
			average hydrodynamic size <sup>b</sup> (nm)	PDI <sup>c</sup> pH 7.5	$\zeta$ potential (mV)	average hydrodynamic size <sup>b</sup> (nm)	PDI <sup>c</sup>	$\zeta$ potential (mV) pH 7.5
S1	15 146	spherical	211.4 $\pm$ 2.3	0.145 $\pm$ 0.01	-13.2 $\pm$ 4.2	226 $\pm$ 9.1	0.282 $\pm$ 0.01	-33.8 $\pm$ 1.8
S2	30 61	spherical	969.3 $\pm$ 39.5	0.266 $\pm$ 0.01	-13.8 $\pm$ 4.4	1094 $\pm$ 46.4	0.364 $\pm$ 0.04	-32.6 $\pm$ 1.7
S3	20 <sup>d</sup> -250 <sup>e</sup>	rod	1419 $\pm$ 16.6	0.405 $\pm$ 0.08	-15.8 $\pm$ 4.0	1275 $\pm$ 66.6	0.179 $\pm$ 0.02	-33.7 $\pm$ 3.5
S4	30 61	spherical	1049 $\pm$ 146.3	0.823 $\pm$ 0.13	12.3 $\pm$ 0.5	1398 $\pm$ 54.9	0.475 $\pm$ 0.01	-36.4 $\pm$ 3.5
P25	21 55	spherical	256.4 $\pm$ 136.6	0.272 $\pm$ 0.02	-15.2 $\pm$ 5.3	325 $\pm$ 4.1	0.260 $\pm$ 0.01	-33.1 $\pm$ 1.7

<sup>a</sup>All data are presented as mean of three independent characterizations  $\pm$  SD. <sup>b</sup>DLS measurements are the mean of at least 3 runs each containing 20 submeasurements. <sup>c</sup>Polydispersity index (PDI); SSA: specific surface area; and FBS: fetal bovine serum. <sup>d</sup>Minimum Feret diameter. <sup>e</sup>Maximum Feret diameter.

It might cause an imbalance between cellular antioxidants and oxidants, in the favor of oxidants. As a result, the high accumulation of reactive oxygen species (ROS) causes the oxidative stress. Oxidative stress responses are crucial for further pathological effects including genotoxicity, inflammation, and fibrosis. Previous studies have shown that relatively large surface areas/particle size have a critical role in increased incidence of lung injury and pulmonary inflammation.<sup>12,13</sup> Specifically, aerodynamic diameter of inhaled particles strongly influences particles deposition to occur in different regions of the human respiratory tract<sup>14</sup> and can cause different biological effects depending on the anatomic target of the human respiratory tract (alveolar or tracheobronchial area) where they accumulate.<sup>15</sup> Studies have also reported that the NP shape could affect toxicity during endocytosis or phagocytosis, for example, the endocytosis of spherical NPs is a more favorable process than that of rod-shaped NPs.<sup>16,17</sup> Nonetheless, spherical NPs are usually less toxic than rod-shaped NPs.<sup>18-20</sup> Although there is growing scientific evidence about TiO<sub>2</sub>-NPs toxicological and even pathological properties,<sup>21</sup> the question of how the physicochemical features of TiO<sub>2</sub>-NPs impact their *in vitro* toxicity has not yet been fully addressed, especially to foster a safer-by-design approach to NP production. Indeed, a safer-by-design approach aims at developing functional as well as safe NMs from their conception, while current NMs are regarded as intrinsically unsafe. The main objective of this approach is to know what property makes a NM or nanoproduct more or less safe.<sup>22</sup> Subsequent steps involve the application of this knowledge to industrial innovation processes, and as a result, NPs that are safer to human and environment are produced. The key factor in this regard is the comprehensive study of the toxicological effects of the physicochemical properties of NPs.<sup>23</sup>

As TiO<sub>2</sub>-NPs could be hazardous, for NP safety and for defining an adequate risk assessment, in particular to protect exposed workers and general population subjects, it is necessary to study how the physical and chemical properties of TiO<sub>2</sub>-NPs determine their biological effects.<sup>24,25</sup>

As one of the main exposure routes to these NPs is inhalation, in this study we aimed to determine the impact of physicochemical properties of TiO<sub>2</sub>-NPs on their *in vitro* toxicity on human lung cell lines. The A549

carcinoma epithelial cell line was used as a monoculture system. A co-culture system consisting of A549 and macrophages (differentiated from the human monocytic THP-1 cell line) was also used as an extended approach to reflect the interactions between different cell types in the lung after exposure to NPs. To that purpose, we thoroughly characterized five types of TiO<sub>2</sub>-NPs with different and well-controlled physicochemical properties: a commercially available P25 sample and four custom-made TiO<sub>2</sub> samples. After exposure, the cell response was assessed in terms of cell viability, proinflammatory response, and oxidative stress status.

## 2. MATERIAL AND METHODS

### 2.1. Physicochemical Characterization of TiO<sub>2</sub> Nanoparticles.

In this study, we used five types of TiO<sub>2</sub>-NPs with different and well-controlled physicochemical properties. In addition to P25 NPs (Evonik P25 CAS: 1317-70-0, Sigma-Aldrich, Saint-Quentin-Fallavier, France), used as a reference, four types of TiO<sub>2</sub>-NPs samples differing in size, shape, agglomeration state, and surface functionalization/charge were synthesized and were named S1–S4 as shown in Table 1.

TiO<sub>2</sub>-NPs were synthesized using Chen *et al.*<sup>26</sup> method. Basically, titanium(IV) butoxide (CAS: 5593-70-4 reagent grade 97%, Sigma-Aldrich, Saint-Quentin-Fallavier, France) was mixed with triethanolamine (CAS: 102-71-6, analytical reagent 97%, VWR International, Fontenay-sous-Bois, France) in 1:2 molar ratio. The mixture was put in a Teflon-lined sealed autoclave and then heated at 150 °C during 24 h. The pH values of the synthesis medium were adjusted using HCl or NH<sub>4</sub>OH to tune particle size and morphology. Finally, the solutions were washed by three centrifugations using deionized water, and the resulting products were dried in an oven at 40 °C. Surface functionalization of S2 NPs was generated by aminopropyltriethoxysilane (APTES) using Zhao *et al.*<sup>27</sup> method. Briefly, 0.25 g of S2 nanopowder was dispersed in 25 mL of deionized water by ultrasonication for 10 min. Then, the silane coupling agents APTES were added in the dispersion (molar ratio of 1:1). The mixture was sonicated until a clear solution was obtained and then refluxed at 80 °C for 4h. After that, dispersed particles were separated from solvent by centrifugation (10 min at 1200 *g*) followed by washing with water at least 2 times. The final functionalized samples were then prepared in deionized water and labeled as S4. The features of NPs are reported in Figure 1 and Table 2.

Stock suspensions of all NPs (1600 µg/mL) were prepared in deionized water (Milli-Q systems, Millipore, Bedford, MA, USA) and sonicated with Branson Sonifier S-450 for 10 min at 89% amplitude. Before each physicochemical measurement and toxicity experiment, stock suspensions were sonicated for 15 min in a bath sonicator and vortexed vigorously, and fresh dilutions were prepared in low light conditions (*i.e.*, 1 µW/cm<sup>2</sup> irradiation intensity) by using Dulbecco's modified Eagle medium (DMEM) to achieve the following final concentrations: 15, 30, 60, and 120 µg/mL. The pH of solutions was measured using a Metrohm digital pH meter of model 827.

The morphology and size distribution of NPs were analyzed by transmission electron microscopy (TEM) using a FEI TECNAI 20FST operating at 200 kV and scanning electron microscopy (SEM) at 2–3 kV on a Zeiss Sigma 300 microscope using a secondary electron (SE) detector. After each TEM image of each sample were chosen, the size distribution and the mean diameter were measured by ImageJ software. The hydrodynamic size and the agglomeration status of TiO<sub>2</sub>-NPs (120 µg/mL) in deionized water and in DMEM were determined by using dynamic light scattering (DLS, Zetasizer Nano ZS Malvern Instruments,

Worcestershire, UK) measurements. Surface charge of the NPs was monitored using electrophoretic light scattering (ELS, Zetasizer Nano ZS Malvern Instruments, Worcester- shire, UK). Specific surface areas (SSA) were measured by linearizing the physisorption isotherm of N<sub>2</sub> at 77 K with the classical method of Brunauer, Emmett, and Teller (BET) (Volumetric Adsorption ASAP 2020, Micrometrics, USA).<sup>28</sup>

Raman spectroscopy (Horiba Jobin–Yvon Xplora spectrometer) and X-ray diffraction (XRD, Miniflex, Rigaku, Japan) techniques were used for the structural identification of the crystalline phases of NPs. Raman spectra were recorded on a system equipped with a confocal microscope and a nitrogen-cooled CCD detector. The high-resolution XRD patterns were measured in the continuous scan mode using a step width of 0.05° (2 $\theta$ ). The scan range was 20–80°. Further parameters of the diffractometer were: Ni filtered K- $\beta$  radiation; voltage 40 kV; tube current 15 mA; scan speed 4° min<sup>-1</sup>.

The spin trapping technique (5-5'-dimethyl-1-pyrroline-*N*-oxide, DMPO, as trapping agent) associated to the electron spin resonance (ESR) spectroscopy (Miniscope 100 ESR spectrometer, Magnettech, Germany) was used to assess whether TiO<sub>2</sub>-NPs have the potential to generate free radicals (hydroxyl and carboxyl radical) under the same laboratory light conditions used for administration to cells. TiO<sub>2</sub> samples (120  $\mu$ g/mL) were suspended in a buffered solution (potassium phosphate buffer 0.25 M, pH 7.4) containing 0.04 M DMPO or 0.04 M DMPO and 1 M sodium formate to detect hydroxyl and carboxyl radicals, respectively. The reaction mixtures were prepared under laboratory light conditions and then kept in the dark at 37 °C. ESR spectra were recorded on aliquots (50  $\mu$ L) withdrawn after 5, 10, 20, and 30 min of incubation. The instrument settings were as follows: microwave power 10 mW; modulation 1000 mG; scan range 120 G; center of field 3345 G. Blanks were performed with the same reaction mixtures without TiO<sub>2</sub>. A suspension of P25, irradiated with a UV lamp for 30 min (100 W, 365 nm UV light, Cole- Parmer, Paris, France), was used as positive control. The irradiation intensity was 1 mW/cm<sup>2</sup> as measured by a radiometer (Model PCE- UV34, PCE Instruments UK Ltd., Southampton, UK). All experi- ments were repeated at least twice.

The presence of Al, Sb, Hg, Pb, Fe, Zn, As, and Cd impurities in TiO<sub>2</sub> samples was determined by Agilent 7800 inductively coupled plasma mass spectrometry (ICP-MS) as recommended by national and international standards (European Commission Directive 95/45/ EC, Food and Drug Administration (FDA) Regulation 21- CFR, European Pharmacopoeia, Pharmacopoeia of the USA, *etc.*) that have set limiting values for the contents of these eight element impurities in TiO<sub>2</sub> samples.<sup>29</sup>

## 2.2. Limulus Amebocyte Lysate Assay: Endotoxin Contamination Assessment.

The amount of endotoxin present in the NP solutions was determined by the chromogenic method with a ToxinSensor Chromogenic Limulus Amebocyte Lysate (LAL) Endotoxin Assay kit (Genscript, Piscataway, Associates of Cape Cod Inc., Falmouth, MA, USA) according to the manufacturer's instructions. All samples were prepared in endotoxin-free vials. The optical density was read at 545 nm. The amount of endotoxin in samples was calculated by comparison with a standard curve of endotoxin. Endotoxin concentrations were expressed as endotoxin units per milligram (EU/mg) of NPs.

## 2.3. Cell Culture.

The A549 human carcinoma epithelial cell line was supplied by the American Type Culture Collection

(ATCC, CCL-185). The THP-1 human monocytic leukemia monocyte cell line (ATCC, TIB-202) was a generous gift from Dr Ghislaine Lacroix from French National Institute for Industrial Environment and Risks (INERIS). A549 cells were used either as a monoculture or co-culture with macrophages differentiated from THP-1 cells (10 A549:1 differentiated-THP-1 ratio).

A549 cells were grown in DMEM supplemented with 10% (v/v) fetal bovine serum (FBS, S1810; Biowest, Nuaille, France) and 1% penicillin-streptomycin (VWR International, Fontenay-sous-Bois, France). A549 cells were grown in flasks, and after reaching 80% confluency, cells were trypsinized, washed with sterile phosphate-buffered saline (PBS), and centrifuged at 1500 g for 10 min and subcultured. The flasks were stored at 37 °C in a humidified atmosphere with 5% CO<sub>2</sub>.

THP-1 was cultured in Roswell Park Memorial Institute (RPMI) 1640 (Gibco, Life Technologies, Cergy-Pontoise, France) containing 10% FBS and 1% penicillin-streptomycin. THP-1 cells were counted with Trypan blue regularly and subcultured usually twice a week. Subcultures were started with a cell concentration of 2 × 10<sup>5</sup> to 4 × 10<sup>5</sup> viable cells/mL, and cells were maintained at a concentration between 10<sup>5</sup> and 10<sup>6</sup> cells/mL in suspension. THP-1 cells were maintained in a humidified atmosphere containing 5% CO<sub>2</sub> at 37 °C. For the co-culture, THP-1 cells were differentiated into mature macrophage-like cells in 96-well plate with 30 ng/mL of phorbol myristate acetate (PMA) (P1585, Sigma-Aldrich, Saint-Quentin-Fallavier, France) in RPMI for 24 h. After the incubation, cell surface was rinsed two times with DPBS. Then A549 cells were added on top of the differentiated THP-1, and the system was further cultivated for 24 h at a ratio of one differentiated THP-1 cell to 10 A549 cells with direct cell-to-cell contact in DMEM supplemented with 10% (v/v) FBS and 1% penicillin-streptomycin.

#### 2.4. Cell Morphology.

A549 cells and co-culture cells were seeded on 96 well plates (1 × 10<sup>5</sup> cells/well in 50 μL of medium) and were allowed to adhere for 24 h. After 24 h exposure to the highest dose (120 μg/mL) of TiO<sub>2</sub> samples, supernatant was discarded, and cell surfaces were washed with PBS. After, cells were observed using optical microscopy (Leica ICC50 HD, Leica Microsystems, Nanterre, France) at 20× magnification, and pictures were captured.

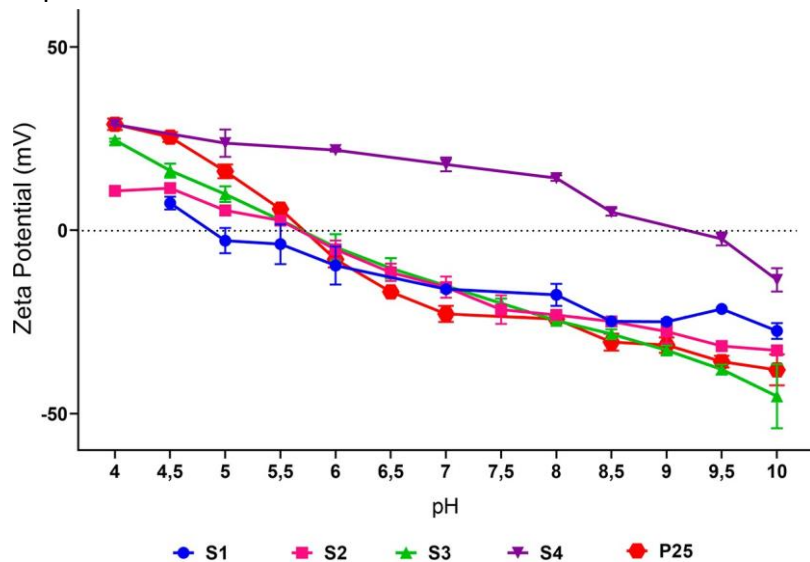


Figure 2. The  $\zeta$  potential vs pH curves of TiO<sub>2</sub>-NPs in 1 mM sodium nitrate (NaNO<sub>3</sub>) solution. Values are the mean  $\pm$  SEM of three independent experiments.

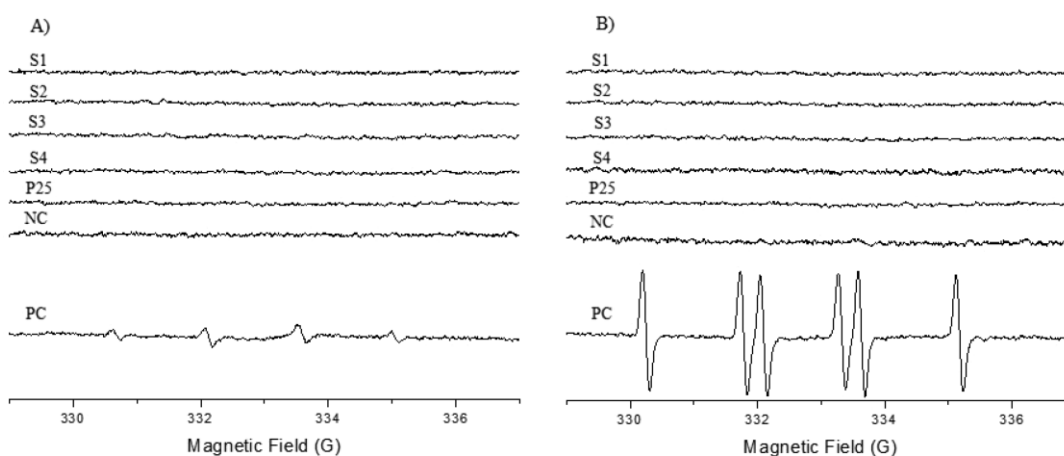


Figure 3. Generation of HO• (A) and CO<sub>2</sub><sup>•-</sup> (B) radicals. Negative control (NC) corresponds to buffer solution without particles. Positive control (PC) corresponds to UV-irradiated P25. The number of radicals produced is proportional to the intensity of the ESR signal.

#### 2.5. Determination of Cell Viability.

Cell viability was determined by Trypan blue exclusion since TiO<sub>2</sub>-NPs have been reported to have interactions with MTT, XTT, and LDH viability assays.<sup>30,31</sup> Trypan blue is a cell membrane-impermeable azo dye that live cells exclude, whereas dead cells do not.  $1.5 \times 10^6$  cells/well were plated onto 6-well microtiter plates in 1000  $\mu$ L culture medium with or without TiO<sub>2</sub>-NPs. After incubation for 24 h at 37 °C in a humidified incubator, the culture medium was removed, and cells were washed with PBS and trypsinized. Twenty  $\mu$ L cell suspensions were mixed with 80  $\mu$ L Trypan blue dye to obtain 1:5 dilution, and cells were counted under a microscope using Thoma cell counting chamber. Results are expressed as the mean of three independent experiments and relative to control (unexposed) cells.

#### 2.6. Proinflammatory Response.

A549 cells and co-culture cells were seeded in 96-well-plates ( $1 \times 10^5$  cells/well in 50  $\mu$ L of medium) and were allowed to adhere for 24 h. NPs were diluted in DMEM cell culture medium to reach the following final concentrations: 15, 30, 60, and 120  $\mu$ g/mL. After 24 h cell exposure to TiO<sub>2</sub>-NPs, the production of tumor necrosis factor alpha (TNF- $\alpha$ ) was evaluated in a co-culture using a commercial ELISA Kit (Quantikine Human TNF- $\alpha$  Immunoassay; R&D Systems, Lille, France) according to the manufacturer's instructions. Interleukin-8 (IL-8) production was assessed in the two cell systems (A549 cells and A549/differentiated-THP-1 co-culture) after exposure to TiO<sub>2</sub>-NPs for 24 h by a commercially available ELISA kit (Quantikine Human IL-8 Immunoassay; R&D Systems, Lille, France) according to the manufacturer's instructions. The optical density of each sample was determined using a microplate reader (Multiskan RC; Thermo Labsystems, Helsinki, Finland) set to 450 nm. Three independent experiments were performed, and the production of TNF- $\alpha$  and IL-8 was reported to that of control (unexposed) cells.

#### 2.7. Determination of Reactive Oxygen Species Production.

A549 cells and co-culture cells were seeded in 96-well black polystyrene microplates ( $1 \times 10^5$  cells/well in  $50 \mu\text{L}$  of medium) and were allowed to adhere for 24 h before assay. After 90 min and 24 h exposure to 15, 30, 60, and  $120 \mu\text{g/mL}$   $\text{TiO}_2$ -NPs, the level of ROS was determined using the OxiSelect kit from Cell Bio Laboratories (San Diego, CA, USA) according to the manufacturer's instructions. Fluorescence was detected using a Fluoroskan Ascent fluorometer (excitation: 480 nm, emission: 530 nm, Thermo Labsystems), and the generation of ROS was reported to that of control (unexposed) cells.

### 2.8. Statistical Analyses.

Statistical analyses were performed using GraphPad Prism (version 8.0, GraphPad Software, San Diego, CA, USA). All data were presented as mean  $\pm$  standard error of the mean (SEM). Differences were considered to be statistically significant when  $P$  value was  $<0.05$ . One-way Anova Tukey test analysis was performed for comparison between control and experimental groups and among experimental groups.

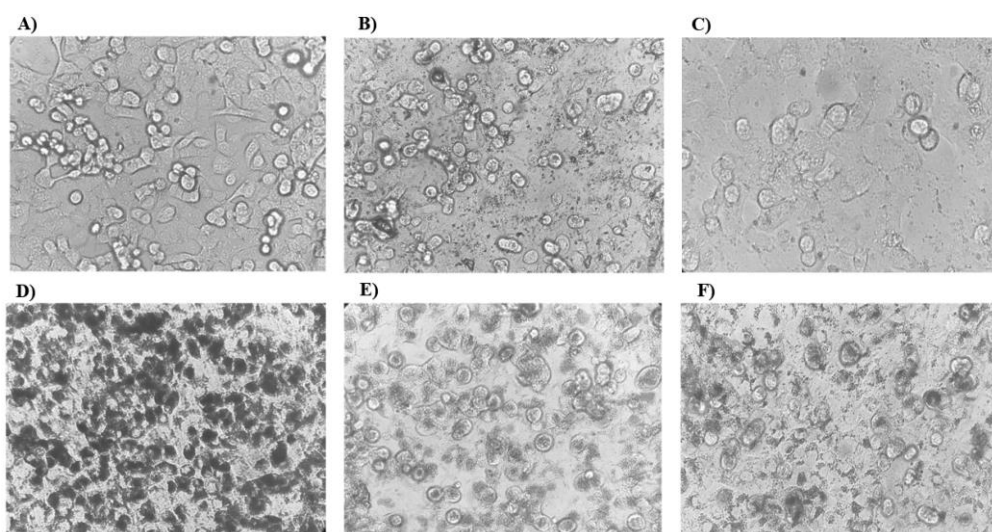


Figure 4. Microscopic images of A549 cells exposed to  $120 \mu\text{g/mL}$   $\text{TiO}_2$ -NPs for 24 h (20 $\times$  magnification). (A) Control cells (unexposed to NPs), (B) S1, (C) S2, (D) S3, (E) S4, and (F) P25.

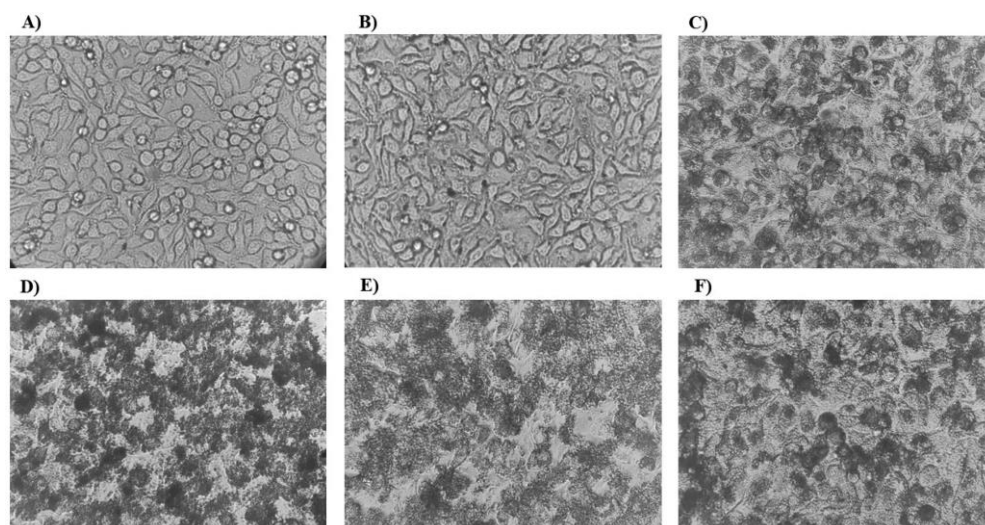


Figure 5. Microscopic images of co-culture cells exposed to 120  $\mu\text{g}/\text{mL}$   $\text{TiO}_2$ -NPs for 24 h (20 $\times$  magnification). (A) Control cells (unexposed to NPs), (B) S1, (C) S2, (D) S3, (E) S4, and (F) P25.

### 3. RESULTS

#### 3.1. Physicochemical Features of $\text{TiO}_2$

The physicochemical characterization of five different  $\text{TiO}_2$ - NPs was performed using TEM, SEM, DLS, BET,  $\zeta$ -potential, Raman spectroscopy, XRD, and ICP-MS to provide clear insight into their primary size, hydrodynamic size, shape, specific surface area, surface charge, crystallinity, and chemical composition. The key toxicity-relevant features of the  $\text{TiO}_2$ - NPs are listed in Table 2 with corresponding TEM images shown in Figure 1.<sup>2</sup> charge. The opposite sign of the surface charge of S4 in DINPs was performed using TEM, SEM, DLS, BET,  $\zeta$ -potential, Raman spectroscopy, XRD, and ICP-MS to provide clear insight into their primary size, hydrodynamic size, shape, specific surface area, surface charge, crystallinity, and chemical composition. The key toxicity-relevant features of the  $\text{TiO}_2$ - NPs are listed in Table 2 with corresponding TEM images shown in Figure 1.

Please note that TEM images were shown to illustrate the NP shape, and as surface functionalization is not expected to alter the NP shape, we consider that a TEM picture of S2 is representative of that of S4.

All samples exhibited a negative surface charge up to  $\text{pH} < 5.5$ , while the S4 surface was positively charged in almost all  $\text{pH}$  values investigate ( $\text{pH} < 9.5$ ) (Figure 2). S4 differentiated from the other samples also in DI  $\text{H}_2\text{O}$  at  $\text{pH} 7.5$ , exhibiting a remarkably positive surface charge (Table 2) which is due to  $\text{H}_2\text{O}$  and DMEM may be due to the different adsorption and affinity of protons on the surface of the particle in the culture medium.

Raman spectra and XRD pattern (Supporting Information) of  $\text{TiO}_2$ -NPs confirmed the anatase phase of S1–S4 and anatase-rutile mixed phase (*ca.* 90:10) of P25.

The free radical generation of  $\text{TiO}_2$ -NPs is shown in Figure 3. No ESR spectra of the DMPO- $\text{HO}^\bullet$  and of the DMPO-  $\text{CO}^\bullet$  adducts were observed for the  $\text{TiO}_2$  samples under the same light conditions used in the cellular tests, thus suggesting that the photocatalytic activity of  $\text{TiO}_2$ -NPs is not a parameter that may affect toxicity results in this study.

The trace toxic impurities of Cd, Hg, As, Pb, Sb, and Zn in the tested samples met purity requirements of typical maximum tolerable limits of 0.5, 0.5, 3, 10, 50, and 50  $\text{mg}/\text{kg}$ , respectively. Moreover, all particle samples were tested by endotoxin assay for the possible presence of endotoxin. Endotoxin content was found to be below the detection limit for all the samples. Since the tested NPs did not contain toxic elements and endotoxins, it could be claimed that the possible toxic effects after NP exposure are only caused by  $\text{TiO}_2$ -NPs themselves.

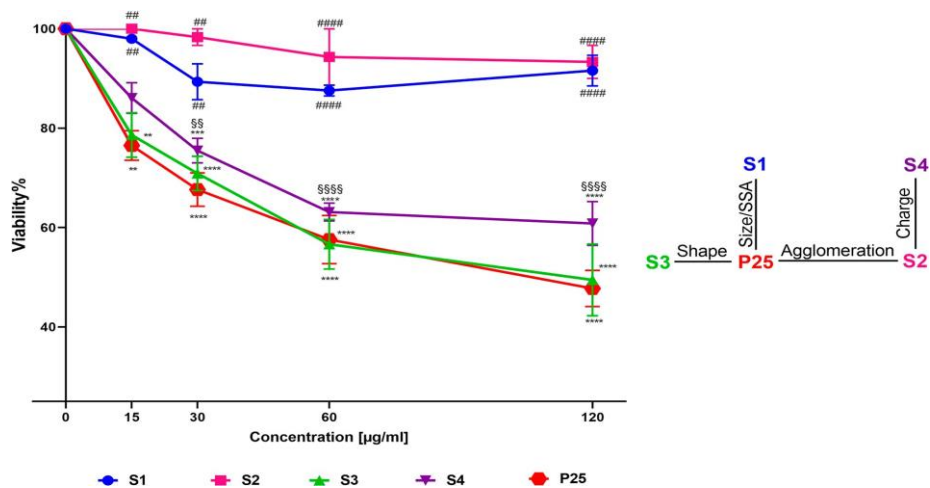


Figure 6. Cell viability assessed by Trypan blue assay 24 h after A549 cells were exposed to TiO<sub>2</sub>-NPs at the indicated concentrations. Values are the mean ± SEM of three independent experiments. Statistically different from control (\*\*)  $P < 0.01$ , (\*\*\*\*)  $P < 0.0001$ . Statistically different from P25 (##)  $P < 0.01$ , (####)  $P < 0.0001$ . Statistical difference between S2 and S4 (§§)  $P < 0.01$ , (§§§§)  $P < 0.0001$ . Statistical analyses were conducted using one-way Anova analyses, followed by Tukey's multiple comparison test.

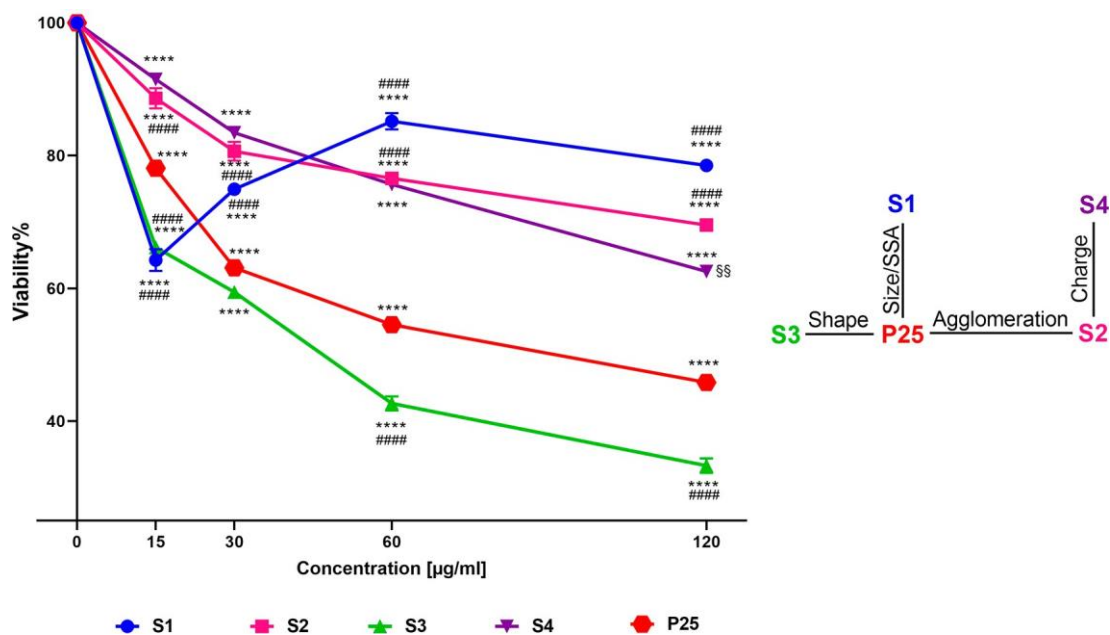


Figure 7. Cell viability assessed by Trypan blue assay 24 h after co-culture cells were exposed to TiO<sub>2</sub>-NPs at the indicated concentrations. Values are the mean ± SEM of three independent experiments. Samples statistically different from control (\*\*\*\*)  $P < 0.0001$ . Statistically different from P25 (#####)  $P < 0.0001$ . Statistical difference between S2 and S4 (§§)  $P < 0.01$ . Statistical analyses were conducted using one-way Anova analyses, followed by Tukey's multiple comparison test.

### 3.2. Cell Morphology.

Figures 4 and 5 illustrate the morphology of A549 cells and A549/differentiated-THP-1 co-cultured cells after 24 h exposure to the highest dose of TiO<sub>2</sub>- NPs (120 µg/mL), respectively. Please note that we chose

the highest NP concentration (120  $\mu\text{g}/\text{mL}$ ) to illustrate the cell morphological changes induced as they were more pronounced in this condition. However, cell morphology alterations were not the same depending on the NP concentration and type. For instance, with the smallest NP concentration, cell morphology was similar to that of control cells. Although such changes should

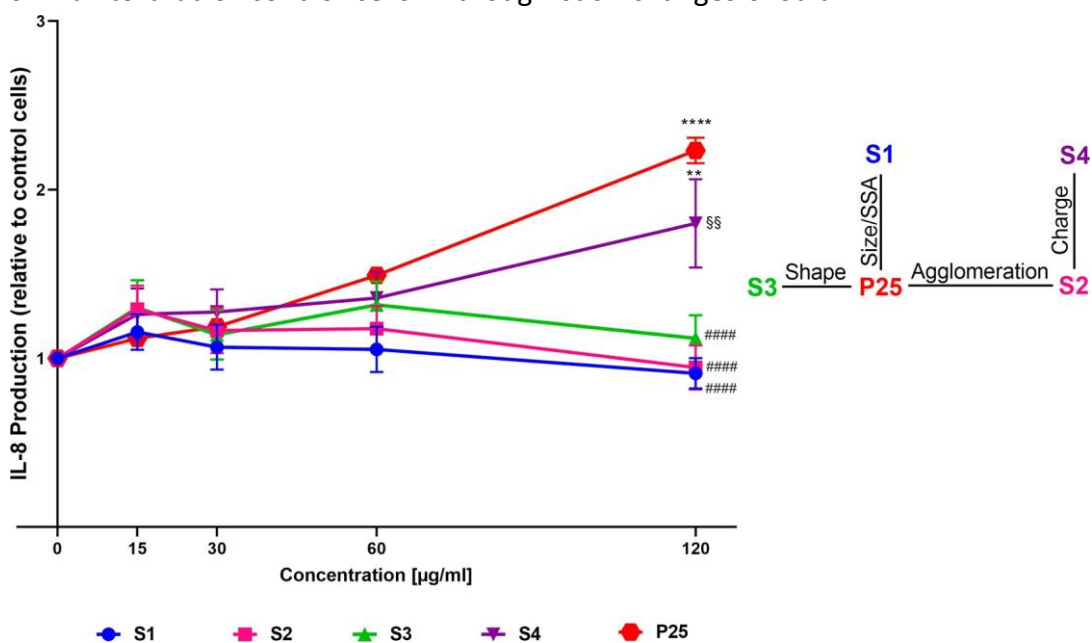


Figure 8. IL-8 production after 24 h exposure to the indicated concentrations of  $\text{TiO}_2$ -NPs in A549 cells. Values are the mean  $\pm$  SEM of three independent experiments. Statistically different from control (\*\*)  $P < 0.01$  and (\*\*\*\*)  $P < 0.0001$ . Statistically different from P25 (#####)  $P < 0.0001$ . Statistical difference between S2 and S4 (§§§§)  $P < 0.01$ . Statistical analyses were conducted using one-way Anova analyses, followed by Tukey's multiple comparison test.

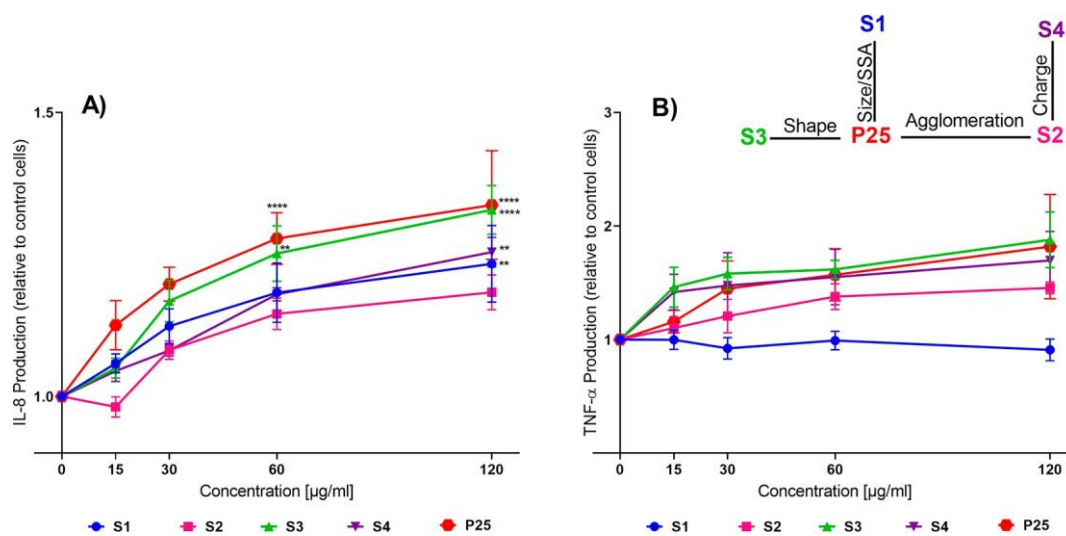


Figure 9. IL-8 (A) and  $\text{TNF-}\alpha$  (B) production after 24 h of exposure to the indicated concentrations of  $\text{TiO}_2$ -NPs in co-culture cells. Values are the mean  $\pm$  SEM of three independent experiments. Statistically different from control (\*\*)  $P < 0.01$  and (\*\*\*\*)  $P < 0.0001$ . Statistical analyses were conducted using one-way Anova analyses, followed by Tukey's multiple comparison test.

### 3.3. Cell Viability.

Cell viability, assessed by Trypan blue, after exposure to TiO<sub>2</sub>-NPs of A549 cells and A549/ differentiated-THP-1 co-culture is reported in Figures 6 and 7, respectively.

In general, a decrease in cell viability was observed after incubating A549 cells with all TiO<sub>2</sub>-NPs, although not statistically significant for S1 and S2. Statistically significant differences were found between P25 and S1, P25 and S2, and S2 and S4.

The co-culture system is considered a more sensitive model than monocultures and better reflect the real tissue environment.<sup>32-34</sup> In co-culture, the tested NPs caused slightly more cell loss than in the A549 cell monoculture. The cell viability decreased in a dose-dependent manner in all samples except S1 (Figure 7). The drastic drop of cell viability at the lowest S1 concentration is quite peculiar. We assume it might be due to experimental artifacts. Direct interaction between NPs and test reagents might cause artifacts; however, there is no evidence that Trypan blue interacts with TiO<sub>2</sub>, unlike MTT and LDH viability tests. Furthermore, artifacts may be a result of unacknowledged impurity (*e.g.*, metal) or endotoxin contamination leading to an overestimation of NP toxicity; however, we assessed toxic element impurity and endotoxin levels and did not observe any contamination. Other possible causes for artifacts include unexpected changes to 15 µg/mL S1 NPs

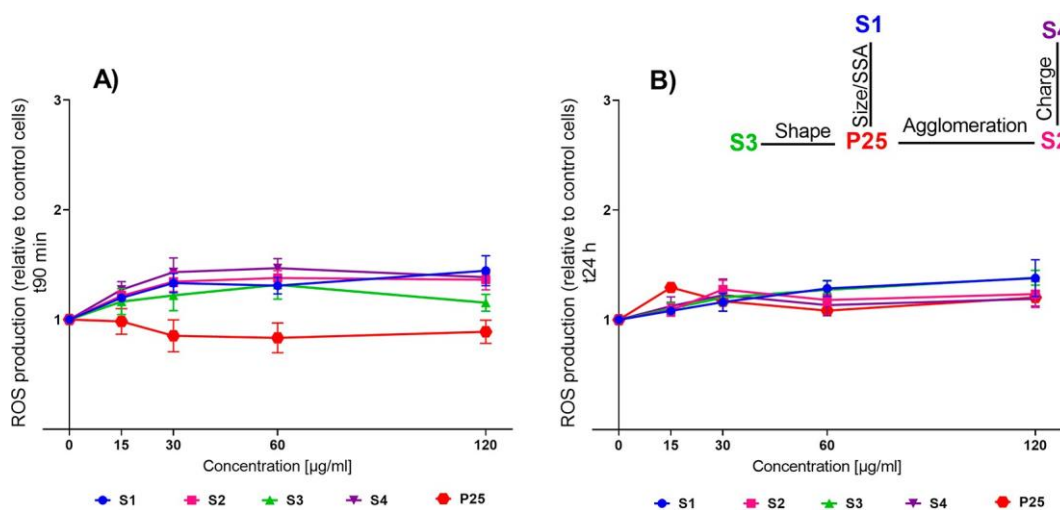


Figure 10. ROS production after 90 min (A) and 24 h (B) exposure to the indicated concentrations of TiO<sub>2</sub>-NPs in A549 cells. Statistical analyses were conducted using one-way Anova analyses, followed by Tukey's multiple comparison test.

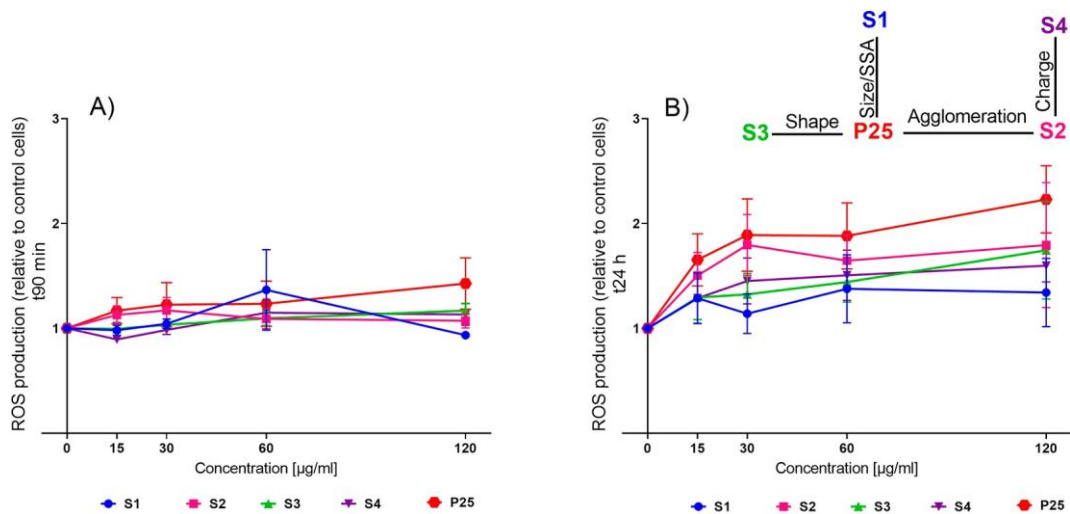


Figure 11. ROS production after 90 min (A) and 24 h (B) exposure to the indicated concentrations of TiO<sub>2</sub>-NPs in co-culture. Statistical analyses were conducted using one-way Anova analyses, followed by Tukey's multiple comparison test.

(dissolution, agglomeration, oxidation, *etc.*) during sample preparation (ultrasonication may cause multiple undesirable and hard to quantify changes) or during testing (settling, dissolution, agglomeration, *etc.*), leading to inaccurate dosing. It is hard to definitively determine the sources of artifacts, and further testing with regard to this aspect is necessary.

The exposure to S3 and P25 induced a higher cell viability loss than S1, S2, and S4. The maximal cell loss was observed for S3. Statistically significant differences were observed when comparing P25 to S1, P25 to S2, and P25 to S3 ( $P < 0.0001$ , all). When comparing S2 to S4, a statistically significant difference was observed only at the highest dose (120 µg/mL,  $P < 0.01$ ).

### 3.4. Proinflammatory Response.

As IL-8 is a major proinflammatory mediator in A549 cells and TNF- $\alpha$  is a proinflammatory cytokine secreted from monocytes/macrophages, IL-8 was assessed for A549, and IL-8 and TNF- $\alpha$  were assessed for the co-cultures. Results are reported in Figures 8 and 9.

In A549 cells, S4 and P25 samples caused a dose-dependent increase in IL-8 production compared to the control group and showed a statistically significant difference at the highest concentration (S4,  $P < 0.01$ ; P25,  $P < 0.0001$ ). When comparing P25 to S1, S2, and S3, only the highest NP concentration (120 µg/mL) induced significant productions of IL-8 ( $P < 0.0001$ , all). When comparing S2 to S4, a statistically significant difference was observed only at the highest dose (120 µg/mL,  $P < 0.01$ ).

In the co-cultures, all samples caused a dose-dependent increase in IL-8 production compared to the control group, although not statistically significant for S2. When the IL-8 production was compared between P25 and the other samples, no statistically significant difference was found.

Except S1, all groups showed a concentration-dependent increase in TNF- $\alpha$  production, although not statistically significant. When compared with P25, no statistically significant difference was found.

### 3.5. Reactive Oxygen Species Production.

Figures 10 and 11 report a ROS production after exposure to the different TiO<sub>2</sub>-NPs of A549 cells and A549/differentiated-THP-1 co- culture, respectively.

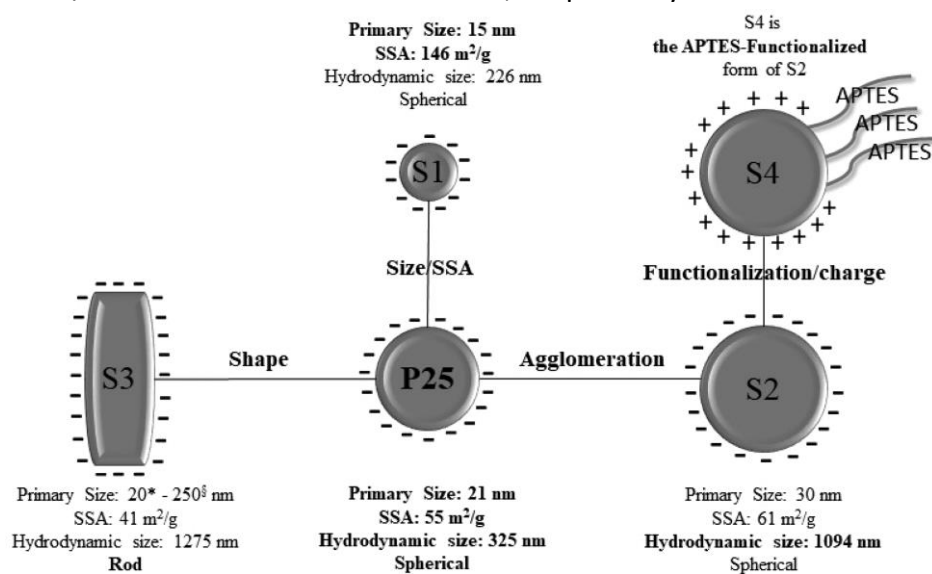


Figure 12. A comparison of NPs with regard to their primary size/SSA, shape, agglomeration state, and surface functionalization/charge (APTES). Particle properties that differ from P25 TiO<sub>2</sub> are reported in bold. (-) Indicates negative surface charge, (+) indicates positive surface charge, \* minimum Feret diameter, and <sup>§</sup> maximum Feret diameter.

Table 3. Impact of TiO<sub>2</sub>-NPs Size and SSA, Shape, Agglomeration State, and Functionalization on their Cytotoxicity<sup>a</sup>

cell viability	impact of the indicated physicochemical features	on A549		A549/differentiated THP-1		proinflammatory effect	oxidative stress	
		as evaluated by comparison between the indicated samples	+	-	+		-	+
<sup>+b</sup> size and SSA	P25 vs S1		+		+	-	-	-
<sup>+b</sup> shape	P25 vs S3		-		+	-	-	-
<sup>+b</sup> agglomeration	P25 vs S2		+		+	-	-	-
<sup>+b</sup> surface charge	S2 vs S4		+		<sup>+b</sup>	-	-	-
-						-	-	-

<sup>a</sup>The + and - indicate an impact or no impact of the physicochemical features on the cytotoxicity respectively. <sup>b</sup>Only at the highest dose.

TiO<sub>2</sub>-NPs did not induce significant ROS production neither in A549 cells nor in co-culture compared to the control group (unexposed to TiO<sub>2</sub>-NPs), whatever the time of analysis (90 min or 24 h).

#### 4. DISCUSSION

As it is commonly acknowledged that the physicochemical properties of NPs (*e.g.*, size, shape, solubility, aggregation, *etc.*) strongly influence their toxicity, we aimed to determine the impact of such features on TiO<sub>2</sub>-NPs toxicity on human lung cell lines. As illustrated by Figure 12 and based on the physicochemical features of the different NPs, by comparing P25 and S1, we were able to highlight the impact of size and SSA on TiO<sub>2</sub>-NPs cytotoxicity. We compared S2 and P25 to investigate the effect of agglomeration on toxicity, as this feature was different between these samples, whereas their primary size, specific surface area, surface charge, and shape were all similar. The influence of particle shape was investigated by comparing rod-shaped S3 with isometric P25 that share similar specific surface areas. Lastly, the surface charge impact on cell response was compared between S2 and S4. It is important to state that the crystalline phases of synthesized NPs and P25 are different from each other in this study. P25 is a mixture of anatase and rutile (approximately 90% anatase and 10% rutile), while other samples have a pure anatase structure. Several studies have shown that anatase is more toxic than similarly sized rutile TiO<sub>2</sub>-NPs.<sup>35-37</sup> Therefore, we can confidently affirm that the anatase phase might be more responsible than the rutile phase for the toxic manifestations that P25 may create. A summary of our observations is reported in Table 3.

As highlighted in the Introduction, a safer-by-design approach cannot be achieved without knowing the impact of physicochemical properties of NPs on their toxicity. In the R&D phase of the safer-by-design approach, the assessment of the hazard profile of NPs exhibiting different physicochemical properties is the first step for avoiding their adverse effects.<sup>38</sup> The results obtained in this study (as summarized in Table 3 and further discussed below) provide data for the design and development of safer TiO<sub>2</sub>-NPs.

##### 4.1. Size and Surface Area Effects.

To determine the effects of the size and surface area of the TiO<sub>2</sub>-NPs on their cytotoxicity, we compared S1 and P25 NPs, whose agglomeration states in the culture medium were very similar. Generally, P25 (21 nm) caused more cell death than smaller sized S1 (15 nm). This finding is consistent with observations at the microscope of cell morphology. Cells were more affected when incubated with P25. P25 also induced a higher IL-8 production in A549 than S1 at the highest NP concentration. Finally, ROS production was similar between P25 and S1. These findings suggest a NP size and surface area impact on cell viability and proinflammatory response, but only at the highest NP concentration. Our findings are consistent with studies showing that size and surface area of NPs might contribute to cytotoxicity.<sup>39,40</sup> In agreement with our finding that larger particles caused more toxicity, Park *et al.*<sup>18</sup> showed that 1  $\mu$ m TiO<sub>2</sub>-Degussa microparticles caused more pronounced morphological changes than smaller 30 nm TiO<sub>2</sub>-NPs in A549 cells. Another study<sup>41</sup> reported that mouse neuroblastoma (Neuro-2A) cells showed a much lower cell viability when incubated with 150 nm nickel ferrite NPs than with 10 nm particles. Pan *et al.*<sup>42</sup> reported that 1.4 nm-sized gold NPs caused more cytotoxicity than 1.2 and 0.8 nm gold NPs on the HeLa cervix carcinoma epithelial cells, SK-Mel-28 melanoma cells, L929 mouse fibroblasts, and mouse monocyte/macrophage cells (J774A1).

However, conflicting results have been reported. For example, exposure to 5 nm TiO<sub>2</sub>-NPs inhibited A549 cell proliferation and led to apoptosis and intracellular ROS production.<sup>43</sup> In another study, 25 nm TiO<sub>2</sub>-NPs

showed greater toxicity than 60 nm TiO<sub>2</sub>-NPs in A549 and 16HBE cells.<sup>44</sup> In addition, Simon-Deckers *et al.* as well as Zhu *et al.* reported that smaller TiO<sub>2</sub>-NPs caused a higher toxicity than bigger ones.<sup>45,46</sup> Therefore, there is no definitive conclusion about the effect of particle size on toxicity. Another example is that 50 nm TiO<sub>2</sub>-NPs caused a greater toxicity than the 6.3, 10, and 100 nm TiO<sub>2</sub>-NPs.<sup>47</sup> Similarly, an interesting finding was that 25 nm TiO<sub>2</sub>-NPs induced more cell death, higher LDH release, and ROS production than 5 and 100 nm TiO<sub>2</sub>-NPs in mouse macrophages.<sup>48</sup> Therefore, toxic effects of TiO<sub>2</sub>-NPs may be related to their structural characteristics as suggested by Zhang *et al.*<sup>48</sup> More mechanistic studies are needed to clarify the NP size impact on cytotoxicity.

Regarding the production of ROS, Jiang *et al.*<sup>49</sup> reported an S-shaped curve for ROS generation per unit surface area within a certain size range (4–195 nm) of TiO<sub>2</sub>-NPs. Also, TiO<sub>2</sub>-NPs below 10 nm or above 30 nm produced similar levels of ROS per surface area, while a sharp increase was observed from 10 to 30 nm. ROS production was clearly observed in A549 cells in two studies<sup>45,50</sup> whatever the size, crystal phase, and shape of TiO<sub>2</sub>-NPs, which were studied in conditions very similar to ours (same cellular model: A549 cells exposed to various types of TiO<sub>2</sub>-NPs, for 24 h at 100 µg/mL). Especially, intracellular ROS production started as early as after 15 min of exposure to P25.<sup>50</sup> However, in our study, TiO<sub>2</sub>-NPs did not trigger the production of ROS whatever the size and surface area. This must be confirmed by a comprehensive study of the oxidative stress also including the assessment of antioxidant systems induction.

#### 4.2. Shape Effects.

When comparing rod-shaped S3 and spherical P25 NPs, we observed that S3 NPs caused more cell death than P25 in co-cultures, suggesting an impact of NP shape on cell viability. However, NP shape had no impact on ROS production and did not seem to influence the proinflammatory response as in co-cultures P25 and S3 induced similar IL-8 and TNF-α productions. Only in A549 cells, P25 caused more IL-8 production than S3 but at the highest NP concentration.

A limited number of studies have considered how the shape of NPs impacts on their toxicity,<sup>20,51,52</sup> and only few papers reported about a specific shape effect of TiO<sub>2</sub>-NPs.<sup>53,54</sup> Gea *et al.*<sup>53</sup> investigated the cytotoxicity of TiO<sub>2</sub>-NPs of three different shapes (bipyramids, rods, platelets) on human bronchial epithelial cells (BEAS-2B) in the presence or absence of light. They observed that in the presence of light, rod-shaped TiO<sub>2</sub> were more cytotoxic than bipyramids and platelets; the latter showing a similar profile of toxicity. However, in the absence of light, platelets induced a higher cytotoxicity than bipyramids and rods. In an *in vivo* study,<sup>54</sup> male Sprague–Dawley rats were exposed to sphere anatase/ rutile P25, sphere pure anatase TiO<sub>2</sub>, and nanobelts pure anatase TiO<sub>2</sub> by intratracheal instillation. Only nanobelts were able to induce inflammation *in vivo*. Studies using other NP types could be mentioned to illustrate the NP shape influence on cytotoxicity. For example, rod-shaped Fe<sub>2</sub>O<sub>3</sub> NPs were found to produce much higher levels of lactate dehydrogenase (LDH) leakage, inflammatory response, and ROS production than sphere Fe<sub>2</sub>O<sub>3</sub> NPs in RAW 264.7.<sup>52</sup> On the contrary, Forest *et al.*<sup>20</sup> reported that rod-shaped CeO<sub>2</sub> NPs produced more toxic effects in terms of LDH release and TNF-α production than octahedron or cubic CeO<sub>2</sub> NPs in RAW 264.7 cells. On the other hand, some studies did not report any effect of NP shape on their cytotoxicity. For instance, Zhao *et al.*<sup>55</sup> did not find a significant difference in the toxicity of rod and sphere mesoporous silica NPs on human colorectal adeno- carcinoma (Caco-2) cells.

The discrepancies described above can be explained by the fact that besides the shape of the NPs, NPs' interaction forces which are different for each type of particle may also affect biological responses, for

example, interparticle van der Waals forces of rod-shaped NPs are larger than those of spherical ones.<sup>56,57</sup> These forces define the ability of NP's cell internalization *via* phagocytosis.<sup>17,58</sup> Meng *et al.*<sup>59</sup> reported that the internalization of rod-shaped silica particles in A549 cells was much higher than that of spherical particles. This may explain why rod-shaped particles caused more cell death in our study. Moreover, when having different attractive forces (van der Waals and others), the tendency to agglomerate in the suspension may also be different.<sup>60</sup> Therefore, it is also difficult to distinguish the shape effect from the agglomeration effect, since agglomeration always occurs in an aqueous system. Finally, due to different cell types, cell sensitivity, and phagocytic activity, it is difficult to compare studies from the literature.

#### 4.3. Agglomeration Effects.

We compared the responses induced by S2 and P25 to determine the effect of agglomeration on toxicity because primary size, surface area, surface charge, and shape of the two particles were all similar, and only their agglomeration state differed. When considering cell viability, highly agglomerated S2 NPs caused less cell death than less agglomerated P25 in both cell systems. Furthermore, IL-8 production was enhanced in the presence of less agglomerated NPs compared to that induced by highly agglomerated NPs in A549 but only at the highest NP concentration. In addition, agglomeration did not affect IL-8 and TNF- $\alpha$  production in co-cultures and had no impact on ROS production.

Magdolenova *et al.*<sup>61</sup> reported that the highly agglomerated TiO<sub>2</sub>-NPs decreased the proliferation activity in Cos-1 monkey kidney fibroblast-like cell line and EUE human embryonic epithelial cells compared to well-dispersed NPs. Large agglomerates of TiO<sub>2</sub>-NPs caused DNA damage, whereas small agglomerates did not. Another study reported that<sup>62</sup> in comparison to large A14 TiO<sub>2</sub>-NP agglomerates, P25 and A60 TiO<sub>2</sub>-NPs that exhibit small and soft agglomerates were more efficiently taken up by the A549 cells, generated more intracellular oxidative stress, and induced a more potent interleukin-8 (IL-8) and monocyte chemotactic protein 1 (MCP-1) proinflammatory response.

There are few *in vivo* studies in the literature which investigated the agglomeration impact of NPs on lung diseases. Noëlet *et al.*<sup>63</sup> exposed male CDF (F344)/CrIBR rats to aerosolized nano-TiO<sub>2</sub>. In groups exposed to large agglomerates (>100 nm), an increase in the number of neutrophils, an indicator of lung inflammation, was observed. However, no increase in other inflammation markers (IL-1 $\alpha$ , IL-6, and TNF- $\alpha$  production) was observed. Exposure to small agglomerates (<100 nm) caused more cell death and ROS production than large agglomerates. Although these results are in agreement with ours, at least regarding cell viability, it is difficult to compare *in vivo* and *in vitro* studies because of a different agglomeration status of NPs that can occur *in vitro* (in culture medium) and *in vivo* in lung fluids. The protein corona forming around the NPs may also have a strong impact on agglomeration and on the subsequent cell/NP interactions.<sup>64</sup>

#### 4.4. Surface Charge Effects.

When the impact of NP surface charge on cell viability was examined, it was observed that positively charged S4 NPs (APTES-functionalized) caused slightly more cell loss than S2, their nonfunctionalized, negatively charged counterparts. However, they exhibited a similar profile of proinflammatory response and oxidative stress, suggesting no impact of this functionalization on proinflammatory response and oxidative stress. Since it is well documented that positively charged NPs have a high affinity for negatively charged cell membrane protein,<sup>65</sup> it is more likely to have a destructive effect on cell membranes. In a study,<sup>66</sup> TiO<sub>2</sub>-NPs bearing -OH, -NH<sub>2</sub>, or -COOH surface groups were evaluated for their effect on

several cancer cells and control cell cytotoxicity. Specifically,  $-NH_2$  and  $-OH$  groups exhibited a significantly higher toxicity than  $-COOH$  on Lewis lung carcinoma and on a prostate cancer cell line isolated from Copenhagen rats. In some studies on other APTES-functionalized NPs, for instance, the cytotoxicity of APTES-functionalized mesoporous and nonporous silica NPs was investigated on RAW 264.7 macrophages.<sup>67</sup> They both induced very low levels of toxicity. Also, these particles did not cause any ROS production, similar to our results. Chavez *et al.*<sup>68</sup> reported that APTES-functionalized luminescent upconversion NPs were found noncytotoxic to HeLa and DLD-1 human colorectal adenocarcinoma cells. Petushov *et al.*<sup>69</sup> showed that 30 nm APTES-functionalized silicalite NPs did not significantly change LDH release activity in HEK293 embryonic kidney cells and in RAW264.7 cells.

Besides the observation of the impact of the NPs physicochemical properties on their toxicity, another main finding of this study was that the co-culture model seemed more sensitive to the adverse effects of  $TiO_2$ -NPs than the monoculture model. It may be due to different uptake levels of NPs in monoculture and co-culture cells. Co-culture cells may show a stronger barrier compared to monoculture due to intercellular bonds and interactions. In a tetra-culture model consisting of A549 + THP-1 + HMC-1 + EAhy926 cells, only phagocytic THP-1 cells have been shown to internalize 50 nm silica particles.<sup>70</sup> Due to cell interaction through cytokines and chemokines, the uptake in one cell type may affect the reaction of the other cell types in the same culture. This can lead to differences in the uptake mechanisms of NPs compared to monoculture. However, in our study, further investigations are needed to support this hypothesis. On the other hand, the fact that co-culture is more sensitive to the toxic effects of NPs may result from different behaviors of cells in the co-culture. Data showed that when co-cultured with A549 cells, THP-1-derived macrophages (M0) differentiated toward the M1- and M2- macrophage phenotype. Therefore, the co-culture of THP-1-derived macrophages with A549 leads to the release of higher levels of proinflammatory cytokines compared to levels observed in the medium of THP1-derived macrophages.<sup>71</sup> In this case, a strong protection of A549 cells provided by THP-1 cells against toxic agents in co-culture has been reported. However, in order to mimic aerosol accumulation in the air space of the lung, direct cell culture may have some limitations given the weak interactions of the cells.<sup>72</sup> Also, different proliferation rates of the co-cultured cells may present a problem and limit the use of co-cultures. The multiple cell cultures represent an improvement compared with single cell cultures and more closely resemble the *in vivo* situation, yet they are still limited to the cells investigated. Thus, co-culture cell model may be considered as essential for developing a predictive *in vitro* model of the lung.

## 5. CONCLUSION

As reported in Table 3, the main effects observed in this study were an impact of  $TiO_2$ -NP size/SSA, shape, agglomeration state, and surface functionalization/charge (APTES) on cell viability in co-cultures. This model seems more sensitive than the A549 monocultures. The same features seemed to have an impact on the proinflammatory response, but only in A549 cells cultivated alone and only at the highest NP concentration. No impact was observed on ROS production. The effect on toxicity was higher in bigger sized, less agglomerated particles and rod-shaped and positively charged particles. Although further investigations are needed, the present study contributes to a better characterization of  $TiO_2$ -NP toxicity by the systematic evaluation of their adverse effects on human lung cell lines in relation to their physicochemical properties. Moreover, such results could open promising perspectives, especially in the context of a safer-by-design approach.

## 6. REFERENCES

- Fujishima, A., Rao, T. N., and Tryk, D. A. (2000) Titanium Dioxide Photocatalysis. *J. Photochem. Photobiol., C 1* (1), 1–21.
1. Chen, X., and Selloni, A. (2014) Introduction: Titanium Dioxide (TiO<sub>2</sub>) Nanomaterials. *Chem. Rev.* *114* (19), 9281–9282.
  2. (2015) *Mineral Commodity Summaries*, p 196, U.S. Geological Survey, Reston, VA..
  3. Weir, A., Westerhoff, P., Fabricius, L., Hristovski, K., and Von Goetz, N. (2012) Titanium Dioxide Nanoparticles in Food and Personal Care Products. *Environ. Sci. Technol.* *46* (4), 2242–2250.
  4. Wang, Y., He, Y., Lai, Q., and Fan, M. (2014) Review of the Progress in Preparing Nano TiO<sub>2</sub>: An Important Environmental Engineering Material. *J. Environ. Sci. (Beijing, China)* *26*, 2139–2177.
  5. Piccinno, F., Gottschalk, F., Seeger, S., and Nowack, B. (2012) Industrial Production Quantities and Uses of Ten Engineered Nanomaterials in Europe and the World. *J. Nanopart. Res.* *14* (9), 1109.
  6. Shi, H., Magaye, R., Castranova, V., and Zhao, J. (2013) Titanium Dioxide Nanoparticles: A Review of Current Toxicological Data. *Part. Fibre Toxicol.* *10* (1), 15.
  7. Grande, F., and Tucci, P. (2016) Titanium Dioxide Nano- particles: A Risk for Human Health? *Mini-Rev. Med. Chem.* *16* (9), 762–769.
  8. Baranowska-Wójcik, E., Sz wajgier, D., Oleszczuk, P., and
  9. Winiarska-Mieczan, A. (2020) Effects of Titanium Dioxide Nano- particles Exposure on Human Health—a Review. *Biol. Trace Elem. Res.* *193* (1), 118–129.
  10. Albanese, A., Tang, P. S., and Chan, W. C. W. (2012) The Effect of Nanoparticle Size, Shape, and Surface Chemistry on Biological Systems. *Annu. Rev. Biomed. Eng.* *14* (1), 1–16.
  11. Oberdörster, G., Oberdörster, E., and Oberdörster, J. (2005)
  12. Nanotoxicology: An Emerging Discipline Evolving from Studies of Ultrafine Particles. *Environ. Health Perspect.* *113* (7), 823–839.
  13. Oberdörster, G., Ferin, J., and Lehnert, B. E. (1994)
  14. Correlation between Particle Size, in Vivo Particle Persistence, and Lung Injury. *Environ. Health Perspect.* *102*, 173–179.
  15. Braakhuis, H. M., Gosens, I., Krystek, P., Boere, J. A., Cassee, F. R., Fokkens, P. H., Post, J. A., van Loveren, H., and Park, M. V. (2014) Particle Size Dependent Deposition and Pulmonary Inflammation after Short-Term Inhalation of Silver Nanoparticles. *Part. Fibre Toxicol.* *11* (1), 49.
  16. Kuehl, P. J., Anderson, T. L., Candelaria, G., Gershman, B., Harlin, K., Hesterman, J. Y., Holmes, T., Hoppin, J., Lackas, C., Norenberg, J. P., Yu, H., and McDonald, J. D. (2012) Regional Particle Size Dependent Deposition of Inhaled Aerosols in Rats and Mice. *Inhalation Toxicol.* *24* (1), 27–35.
  17. Asgharian, B., and Price, O. T. (2007) Deposition of Ultrafine (NANO) Particles in the Human Lung. *Inhalation Toxicol.* *19* (13), 1045–1054.
  18. Verma, A., and Stellacci, F. (2010) Effect of Surface Properties on Nanoparticlea€“Cell Interactions. *Small* *6* (1), 12–21.
  19. Champion, J. A., and Mitragotri, S. (2006) Role of Target Geometry in Phagocytosis. *Proc. Natl. Acad. Sci. U. S. A.* *103* (13), 4930–4934.
  20. Park, S., Lee, Y. K., Jung, M., Kim, K. H., Chung, N., Ahn, E.-K.,

21. Lim, Y., and Lee, K.-H. (2007) Cellular Toxicity of Various Inhalable Metal Nanoparticles on Human Alveolar Epithelial Cells. *Inhalation Toxicol.* 19 (sup1), 59–65.
22. Hsiao, I.-L., and Huang, Y.-J. (2011) Effects of Various Physicochemical Characteristics on the Toxicities of ZnO and TiO<sub>2</sub> Nanoparticles toward Human Lung Epithelial Cells. *Sci. Total Environ.* 409 (7), 1219–1228.
23. Forest, V., Leclerc, L., Hochepped, J.-F., Trouvé, A., Sarry, G.,  
24. and Pourchez, J. (2017) Impact of Cerium Oxide Nanoparticles Shape on Their in Vitro Cellular Toxicity. *Toxicol. In Vitro* 38, 136– 141.
25. (2006) *IARC Monographs on the Evaluation of Carcinogenic Risks to Humans Carbon Black, Titanium Dioxide, and Talc*, Vol. 93, pp 193–412, International Agency for Research on Cancer, Lyon, France.
26. Fadeel, B. (2013) Nanosafety: Towards Safer Design of Nanomedicines. *J. Intern. Med.* 274 (6), 578–580.
27. Geraci, C., Heidel, D., Sayes, C., Hodson, L., Schulte, P., Eastlake, A., and Brenner, S. (2015) Perspectives on the Design of Safer Nanomaterials and Manufacturing Processes. *J. Nanopart. Res.* 17 (9), 1–13.
28. Shin, S. W., Song, I. H., and Um, S. H. (2015) Role of Physicochemical Properties in Nanoparticle Toxicity. *Nanomaterials* 5 (3), 1351–1365.
29. Iavicoli, I., Leso, V., and Bergamaschi, A. (2012) Toxicological Effects of Titanium Dioxide Nanoparticles: A Review of in Vivo Studies. *J. Nanomater.* 2012, 1.
30. Chen, D. W., Shi, J. E., Yan, J. C., Wang, Y. H., Yan, F. C.,  
31. Shang, S. X., and Xue, J. (2008) Controllable Synthesis of Titania Nanocrystals with Different Morphologies and Application to the Degradation of Phenol. *Chem. Res. Chin. Univ.* 24 (3), 362–366.
32. Zhao, J., Milanova, M., Warmoeskerken, M. M. C. G., and Dutschk, V. (2012) Surface Modification of TiO<sub>2</sub> Nanoparticles with Silane Coupling Agents. *Colloids Surf., A* 413, 273–279.
33. Brunauer, S., Emmett, P. H., and Teller, E. (1938) Adsorption of Gases in Multimolecular Layers. *J. Am. Chem. Soc.* 60 (2), 309– 319.
34. Wang, Z., Ni, Z., Qiu, D., Chen, T., Tao, G., and Yang, P. (2004) Determination of Metal Impurities in Titanium Dioxide Using Slurry Sample Introduction by Axial Viewing Inductively Coupled Plasma Optical Emission Spectrometry. *J. Anal. At. Spectrom.* 19 (2), 273.
35. Wang, S., Yu, H., and Wickliffe, J. K. (2011) Limitation of the MTT and XTT Assays for Measuring Cell Viability Due to Superoxide Formation Induced by Nano-Scale TiO<sub>2</sub>. *Toxicol. In Vitro* 25 (8), 2147–2151.
36. Holder, A. L., Goth-Goldstein, R., Lucas, D., and Koshland, C.  
37. P. (2012) Particle-Induced Artifacts in the MTT and LDH Viability Assays. *Chem. Res. Toxicol.* 25, 1885.
38. Drumm, K., Attia, D. I., Kannt, S., Micke, P., Buhl, R., and Kienast, K. (2000) Soot-Exposed Mononuclear Cells Increase Inflammatory Cytokine mRNA Expression and Protein Secretion in Cocultured Bronchial Epithelial Cells. *Respiration* 67 (3), 291–297.
39. Holownia, A., Wielgat, P., Kwolek, A., Jackowski, K., and Braszko, J. J. (2015) Crosstalk between Co-Cultured A549 Cells and Thp1 Cells Exposed to Cigarette Smoke. *Adv. Exp. Med. Biol.* 858, 47–55.

40. Dehai, C., Bo, P., Qiang, T., Lihua, S., Fang, L., Shi, J., Jingyan, C., Yan, Y., Guangbin, W., and Zhenjun, Y. (2014) Enhanced Invasion of Lung Adenocarcinoma Cells after Co-Culture with THP-1-Derived Macrophages via the Induction of EMT by IL-6. *Immunol. Lett.* 160 (1), 1–10.
41. Uboldi, C., Urban, P., Gilliland, D., Bajak, E., Valsami-Jones, E.,
42. Ponti, J., and Rossi, F. (2016) Role of the Crystalline Form of Titanium Dioxide Nanoparticles: Rutile, and Not Anatase, Induces Toxic Effects in Balb/3T3 Mouse Fibroblasts. *Toxicol. In Vitro* 31, 137–145.
43. Gerloff, K., Fenoglio, I., Carella, E., Kolling, J., Albrecht, C., Boots, A. W., Förster, I., and Schins, R. P. F. (2012) Distinctive Toxicity of TiO<sub>2</sub> Rutile/Anatase Mixed Phase Nanoparticles on Caco-2 Cells. *Chem. Res. Toxicol.* 25 (3), 646–655.
44. Sayes, C. M., Wahi, R., Kurian, P. A., Liu, Y., West, J. L., Ausman, K. D., Warheit, D. B., and Colvin, V. L. (2006) Correlating Nanoscale Titania Structure with Toxicity: A Cytotoxicity and Inflammatory Response Study with Human Dermal Fibroblasts and Human Lung Epithelial Cells. *Toxicol. Sci.* 92 (1), 174–185.
45. Kraegeloh, A., Suarez-Merino, B., Sluijters, T., and Micheletti,
46. C. (2018) Implementation of Safe-by-Design for Nanomaterial Development and Safe Innovation: Why We Need a Comprehensive Approach. *Nanomaterials* 8 (4), 239.
47. Zhang, S., Gao, H., and Bao, G. (2015) Physical Principles of Nanoparticle Cellular Endocytosis. *ACS Nano* 9 (9), 8655–8671.
48. Hoshyar, N., Gray, S., Han, H., and Bao, G. (2016) The Effect of Nanoparticle Size on *in Vivo* Pharmacokinetics and Cellular Interaction. *Nanomedicine* 11 (6), 673–692.
49. Yin, H., Too, H. P., and Chow, G. M. (2005) The Effects of Particle Size and Surface Coating on the Cytotoxicity of Nickel Ferrite. *Biomaterials* 26 (29), 5818–5826.
50. Pan, Y., Neuss, S., Leifert, A., Fischler, M., Wen, F., Simon, U., Schmid, G., Brandau, W., and Jahnen-Dechent, W. (2007) Size-Dependent Cytotoxicity of Gold Nanoparticles. *Small* 3 (11), 1941–
51. 1949.
52. Wang, Y., Cui, H., Zhou, J., Li, F., Wang, J., Chen, M., and Liu,
53. Q. (2015) Cytotoxicity, DNA Damage, and Apoptosis Induced by Titanium Dioxide Nanoparticles in Human Non-Small Cell Lung Cancer A549 Cells. *Environ. Sci. Pollut. Res.* 22 (7), 5519–5530.
54. Ma, Y., Guo, Y., Wu, S., Lv, Z., Zhang, Q., and Ke, Y. (2017)
55. Titanium Dioxide Nanoparticles Induce Size-Dependent Cytotoxicity and Genomic DNA Hypomethylation in Human Respiratory Cells. *RSC Adv.* 7 (38), 23560–23572.
56. Simon-Deckers, A., Gouget, B., Mayne-L’Hermite, M., Herlin-
57. Boime, N., Reynaud, C., and Carrière, M. (2008) *In Vitro* Investigation of Oxide Nanoparticle and Carbon Nanotube Toxicity and Intracellular Accumulation in A549 Human Pneumocytes. *Toxicology* 253 (1–3), 137–146.
58. Zhu, R. R., Wang, S. L., Chao, J., Shi, D. L., Zhang, R., Sun, X.
59. Y., and Yao, S. D. (2009) Bio-Effects of Nano-TiO<sub>2</sub> on DNA and Cellular Ultrastructure with Different Polymorph and Size. *Mater. Sci. Eng., C* 29 (3), 691–696.
60. Braydich-Stolle, L. K., Schaeublin, N. M., Murdock, R. C., Jiang, J., Biswas, P., Schlager, J. J., and Hussain, S. M. (2009) Crystal Structure Mediates Mode of Cell Death in TiO<sub>2</sub> Nanotoxicity. *J. Nanopart. Res.* 11 (6), 1361–1374.

61. Zhang, J., Song, W., Guo, J., Zhang, J., Sun, Z., Li, L., Ding, F., and Gao, M. (2013) Cytotoxicity of Different Sized TiO<sub>2</sub>nanopar- ticles in Mouse Macrophages. *Toxicol. Ind. Health* 29 (6), 523–533.
62. Jiang, J., Oberdörster, G., Elder, A., Gelein, R., Mercer, P., and
63. Biswas, P. (2008) Does Nanoparticle Activity Depend upon Size and Crystal Phase? *Nanotoxicology* 2 (1), 33–42.
64. Jugan, M. L., Barillet, S., Simon-Deckers, A., Herlin-Boime, N., Sauvaigo, S., Douki, T., and Carriere, M. (2012) Titanium Dioxide Nanoparticles Exhibit Genotoxicity and Impair DNA Repair Activity in A549 Cells. *Nanotoxicology* 6 (5), 501–513.
65. Wang, L., Ai, W., Zhai, Y., Li, H., Zhou, K., and Chen, H. (2015) Effects of Nano-CeO<sub>2</sub> with Different Nanocrystal Morphol- ogies on Cytotoxicity in HepG2 Cells. *Int. J. Environ. Res. Public Health* 12 (9), 10806–10819.
66. Lee, J. H., Ju, J. E., Kim, B. Il, Pak, P. J., Choi, E.-K., Lee, H.-S.,
67. and Chung, N. (2014) Rod-Shaped Iron Oxide Nanoparticles Are More Toxic than Sphere- Shaped Nanoparticles to Murine Macro- phage Cells. *Environ. Toxicol. Chem.* 33 (12), 2759–2766.
68. Gea, M., Bonetta, S., Iannarelli, L., Giovannozzi, A. M., Maurino, V., Bonetta, S., Hodoroaba, V. D., Armato, C., Rossi, A. M., and Schiliro, T. (2019) Shape-Engineered Titanium Dioxide Nano- particles (TiO<sub>2</sub>-NPs): Cytotoxicity and Genotoxicity in Bronchial Epithelial Cells. *Food Chem. Toxicol.* 127, 89–100.
69. Silva, R. M., TeeSy, C., Franzi, L., Weir, A., Westerhoff, P., Evans, J. E., and Pinkerton, K. E. (2013) Biological Response to Nano-Scale Titanium Dioxide (TiO<sub>2</sub>): Role of Particle Dose, Shape, and Retention. *J. Toxicol. Environ. Health, Part A* 76 (16), 953–972.
70. Zhao, Y., Wang, Y., Ran, F., Cui, Y., Liu, C., Zhao, Q., Gao, Y., Wang, D., and Wang, S. (2017) A Comparison between Sphere and Rod Nanoparticles Regarding Their in Vivo Biological Behavior and Pharmacokinetics. *Sci. Rep.* 7 (1), 4131.
71. Brown, S. C., Kamal, M., Nasreen, N., Baumuratov, A., Sharma, P., Antony, V. B., and Moudgil, B. M. (2007) Influence of Shape, Adhesion and Simulated Lung Mechanics on Amorphous Silica Nanoparticle Toxicity. *Adv. Powder Technol.* 18 (1), 69–79.
72. Vold, M. J. (1954) Van Der Waals' Attraction between
73. Anisometric Particles. *J. Colloid Sci.* 9 (5), 451–459.
74. Yameen, B., Choi, W., Vilos, C., Swami, A., Shi, J., and Farokhzad, O. C. (2014) Insight into Nanoparticle Cellular Uptake and Intracellular Targeting. *J. Controlled Release* 190, 485–499.
75. Meng, H., Yang, S., Li, Z., Xia, T., Chen, J., Ji, Z., Zhang, H.,
76. Wang, X., Lin, S., Huang, C., Zhou, Z. H., Zink, J. I., and Nel, A. E. (2011) Aspect Ratio Determines the Quantity of Mesoporous Silica Nanoparticle Uptake by a Small Gtpase-Dependent Macropinocytosis Mechanism. *ACS Nano* 5 (6), 4434–4447.
77. Powers, K. W., Palazuelos, M., Moudgil, B. M., and Roberts, S.
78. M. (2007) Characterization of the Size, Shape, and State of Dispersion of Nanoparticles for Toxicological Studies. *Nanotoxicology* 1 (1), 42–51.
79. Magdolenova, Z., Bilanicová, D., Pojana, G., Fjellsbø, L. M.,
80. Hudecova, A., Hasplova, K., Marcomini, A., and Dusinska, M. (2012) Impact of Agglomeration and Different Dispersions of Titanium Dioxide Nanoparticles on the Human Related in Vitro Cytotoxicity and Genotoxicity. *J. Environ. Monit.* 14 (2), 455.
81. Andersson, P. O., Lejon, C., Ekstrand-Hammarström, B., Akfur, C., Ahlinder, L., Bucht, A., and

- Österlund, L. (2011) Polymorph- and Size-Dependent Uptake and Toxicity of TiO<sub>2</sub> Nanoparticles in Living Lung Epithelial Cells. *Small* 7 (4), 514–523.
82. Noël, A., Maghni, K., Cloutier, Y., Dion, C., Wilkinson, K. J., Halle, S., Tardif, R., and Truchon, G. (2012) Effects of Inhaled Nano- TiO<sub>2</sub> Aerosols Showing Two Distinct Agglomeration States on Rat Lungs. *Toxicol. Lett.* 214 (2), 109–119.
84. Forest, V., Cottier, M., and Pourchez, J. (2015) Electrostatic Interactions Favor the Binding of Positive Nanoparticles on Cells: A Reductive Theory. *Nano Today* 10 (6), 677–680.
85. Wilhelm, C., Billotey, C., Roger, J., Pons, J. N., Bacri, J. C., and Gazeau, F. (2003) Intracellular Uptake of Anionic Superparamagnetic Nanoparticles as a Function of Their Surface Coating. *Biomaterials* 24 (6), 1001–1011.
86. Thevenot, P., Cho, J., Wavhal, D., Timmons, R. B., and Tang, L. (2008) Surface Chemistry Influences Cancer Killing Effect of TiO<sub>2</sub> Nanoparticles. *Nanomedicine* 4 (3), 226–236.
87. Lehman, S. E., Morris, A. S., Mueller, P. S., Salem, A. K., Grassian, V. H., and Larsen, S. C. (2016) Silica Nanoparticle- Generated ROS as a Predictor of Cellular Toxicity: Mechanistic Insights and Safety by Design. *Environ. Sci.: Nano* 3 (1), 56–66.
88. Chavez, D. H., Juarez-Moreno, K., and Hirata, G. A. (2016) Aminosilane Functionalization and Cytotoxicity Effects of Upconversion Nanoparticles Y<sub>2</sub>O<sub>3</sub> and Gd<sub>2</sub>O<sub>3</sub> Co-Doped with Yb<sup>3+</sup> and Er<sup>3+</sup>. *Nanobiomedicine* 3, 1.
89. Petushkov, A., Intra, J., Graham, J. B., Larsen, S. C., and Salem, K. (2009) Effect of Crystal Size and Surface Functionalization on the Cytotoxicity of Silicalite-1 Nanoparticles. *Chem. Res. Toxicol.* 22 (7), 1359–1368.
90. Klein, S. G., Serchi, T., Hoffmann, L., Blömeke, B., and Gutleb, C. (2013) An Improved 3D Tetraculture System Mimicking the Cellular Organisation at the Alveolar Barrier to Study the Potential Toxic Effects of Particles on the Lung. *Part. Fibre Toxicol.* 10 (1), 31.
91. Dehai, C., Bo, P., Qiang, T., Lihua, S., Fang, L., Shi, J., Jingyan, C., Yan, Y., Guangbin, W., and Zhenjun, Y. (2014) Enhanced Invasion of Lung Adenocarcinoma Cells after Co-Culture with THP-1-Derived Macrophages via the Induction of EMT by IL-6. *Immunol. Lett.* 160 (1), 1–10.
92. Rothen-Rutishauser, B. M., Kiama, S. C., and Gehr, P. (2005) A Three-Dimensional Cellular Model of the Human Respiratory Tract to Study the Interaction with Particles. *Am. J. Respir. Cell Mol. Biol.* 32 (4), 281–289.
- 93.